The Canadian Mineralogist
Vol. 41, pp. 937-949 (2003)

THE RELATIONSHIP BETWEEN Cu CONTENT AND DISTORTION IN THE ATOMIC STRUCTURE OF MELANTERITE FROM THE RICHMOND MINE, IRON MOUNTAIN, CALIFORNIA

RONALD C. PETERSON§

Department of Geological Sciences and Geological Engineering, Queen's University, Kingston, Ontario K7L 3N6, Canada

ABSTRACT

The crystal structure of four synthetic samples of melanterite, $(Fe,Cu)SO_4 \cdot 7H_2O$, and six natural samples of melanterite and one of zinc-melanterite from the Richmond mine, Iron Mountain, California, has been refined in space group $P2_1/c$. The structure refinements show that substitution of Cu for Fe at the *M*2 site distorts the octahedron in a square-planar fashion. This behavior is attributed to the Jahn–Teller distortion induced by incorporation of Cu^{2+} (d^9) at the *M*2 site. The *M*1 octahedron does not undergo a similar distortion. Chemical analyses for Fe, Cu and Zn by electron microprobe, AA and ICP–MS reveal a wide variation in the chemical composition of melanterite from this locality, but no strong correlation was found between the proportions of Cu, Fe and Zn and the wide range of colors exhibited by the material. Melanterite with a deep blue color could easily be confused with chalcanthite during field observations.

Keywords: melanterite, zinc-melanterite, boothite, crystal structure, Jahn–Teller distortion, Richmond mine, Iron Mountain, California.

SOMMAIRE

La structure cristalline de quatre échantillons synthétiques de mélanterite, $(Fe,Cu)SO_4 \cdot 7H_2O$, et de six échantillons naturels de mélanterite et un de zinc-mélanterite provenant de la mine Richmond, située à Iron Mountain, en Californie, a été affinée dans le groupe spatial $P2_1/c$. Les résultats montrent que la substitution de Cu au Fe au site *M*2 cause une déformation de l'octaèdre pour donner un polyèdre à plan carré. Ce comportement serait dû à une distorsion de type Jahn–Teller à cause de l'incorporation des ions Cu^{2+} (d^9) au site *M*2. En revanche, l'octaèdre *M*1 ne subit aucune déformation semblable. Les analyses de ces échantillons pour le Fe, Cu and Zn avec une microsonde électronique, par absorption atomique et par plasma avec couplage inductif et spectrométrie de masse (ICP–MS) révèlent une variabilité importante en composition chimique de la mélanterite provenant de cet endroit, mais sans forte corrélation entre les proportions de Cu, Fe et Zn, et la couleur du matériau. La mélanterite bleu foncé pourrait facilement passer pour la chalcanthite dans les observations préliminaires sur le terrain.

(Traduit par la Rédaction)

Mots-clés: mélanterite, zinc-mélanterite, boothite, structure cristalline, distortion de Jahn–Teller, mine Richmond, Iron Mountain, Californie.

INTRODUCTION

Sulfate minerals commonly form where water has interacted with sulfide mine waste. These reactions produce acidic solutions that are heavily laden with metals. The composition of the solutions varies as minerals are precipitated and dissolved, as the mine waste responds to external factors such as seasonal variations in temperature and rainfall at the mine site (Alpers *et al.* 1994b). Sulfate minerals are very important in this process, as they provide a diverse group of atomic structures capable of a wide variety of chemical compositions (Hawthorne *et al.* 2000). As mine-waste solutions evolve, many different sulfates may crystallize and dissolve. Each mineral structure incorporates different metals and has a different field of stability with respect to such factors as temperature, pH, relative humidity and metal concentrations.

The main purpose of this work was to study the structural response of the melanterite as Cu substitutes for Fe. Melanterite is commonly one of the first minerals to crystallize as sulfide mine-waste oxidizes and interacts with water. Melanterite has the ability to incorporate many different metals into its structure, and thus affects

§ *E-mail address*: peterson@geol.queensu.ca

the composition of the mine waters from which it crystallizes. Melanterite from Iron Mountain, California, exhibits a wide range of chemical composition and provides an excellent opportunity to study the limits of substitution and changes in atomic structure in response to these chemical variations. It also exhibits a wide spectrum of colors, such as dark green, yellow, light blue and dark blue. In this study, I evaluate the dependence of color on major-element chemistry, and characterize the structural aspects by refinement of the crystal structure of four synthetic samples and seven natural samples.

The Mines at Iron Mountain, California

The mines at Iron Mountain, northern California (Fig. 1), produce extremely acidic mine-waters that are heavily laden with metals (Alpers *et al.*1992, Nordstrom & Alpers 1999). A gossan zone and the underlying massive pyrite orebody have been mined as a source of Au and Cu, as well as pyrite to produce sulfuric acid. The mines contain extensive workings (Fig. 1) through which groundwater percolates and then enters the watershed of the Sacramento River. The melanterite selected for this study was taken from the Richmond mine.

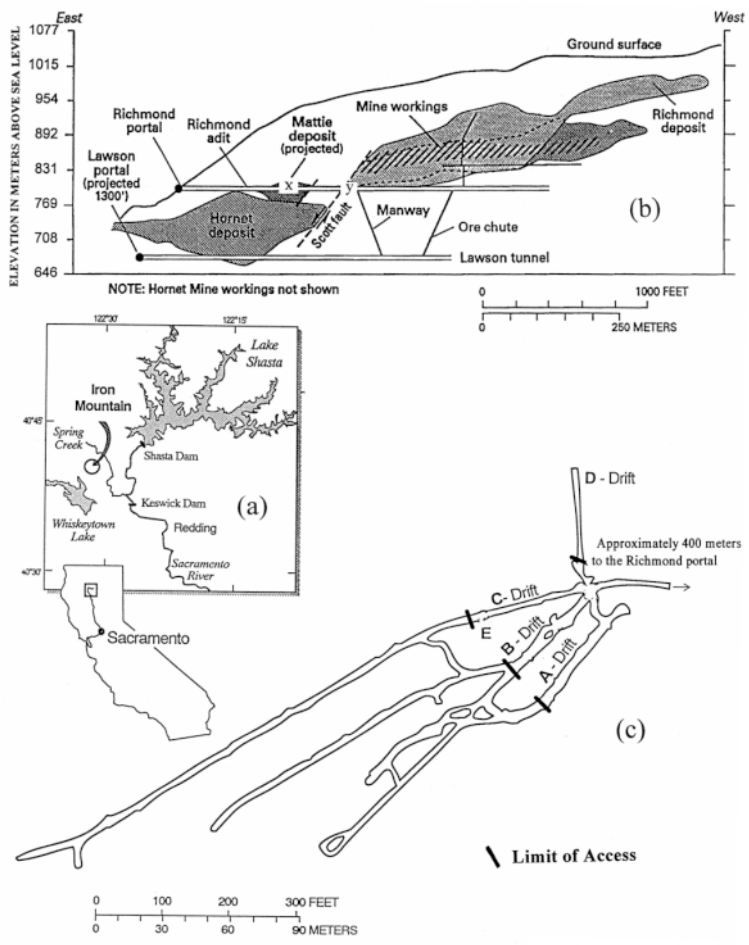

FIG. 1. (a) A map of the state of California, indicating the location of Iron Mountain. (b) A cross-section of the Richmond mine indicating the relative positions of the Richmond and Mattie deposits, taken from Alpers *et al.* (1992) and reproduced with the permission of the U.S. Geological Survey. Access was through the Richmond portal; x marks the location of samples that are described as Mattie deposit samples. Samples from the Richmond deposit were collected at y. (c) Samples from the Richmond deposit were collected from the drifts that meet at the five-way junction. Locations of samples in Figure 6 refer to these drifts.

An adit in the Richmond mine has been maintained and provides a unique opportunity to study the sequence of precipitation and dissolution of minerals and the effect on the resulting effluent. At one point, this adit passes close to the Mattie deposit, where fluids originating from this orebody also precipitate secondary sulfates. The pyrite ore and pyrite-containing waste rock at this mine are highly susceptible to oxidation. There are historical accounts of sulfides contained in ore cars generating extreme heat, to the point of incandescence, upon exposure to air, as the cars were pushed out of the mine. The fluids in the mine are extremely acidic, with pH as low as –3.6 and total concentrations of dissolved solids approaching 1000 g L^{-1} (Alpers *et al.* 1994a, Nordstrom *et al.* 2000). The cycle of arid and wet periods in northern California and the permeability of the deposit create a very dynamic environment ideally suited for the precipitation of secondary sulfates.

The distribution of supergene sulfates within the mine workings is highly variable and depends on temperature, humidity, pH and the availability of oxygen. These parameters vary within the mine and throughout the year (Alpers *et al.* 1994b). Melanterite occurs throughout the mine as a coating on mine walls and as stalactites and stalagmites, which form where fluid drips from the adit roof or from mechanical systems such as pipes and tubes (Figs. 2, 3).

Previous Work

Minerals of the melanterite group ($MSO_4 \cdot 7H_2O$, *M* = Fe, Cu, Zn, Co and Mn) are common in zones of alteration in which sulfide minerals are subject to oxidation (*e.g.*, Frau 2000). Melanterite, with a structure consisting of a flexible array of metal-containing octahedra that are loosely held together by hydrogen bonding, is capable of incorporating a wide range of divalent transition metals. The actual composition of a melanterite-group mineral closely reflects the availability of these metals in the parent solutions; however, experimental work (Fig. 4) by Bodurtha (1995) has shown that in the system $CuSO_4$–$FeSO_4$–H_2O, a partition of cations is established between a crystal and the liquid with which it is in equilibrium. The Fe end-member, melanterite *sensu stricto*, is the most common, and typically is found where pyrite from a coal deposit or a massive sulfide ore has been oxidized. Gaines *et al.* (1997) (and references therein) reviewed the minerals of this group. Jambor *et al.* (2000) described the details of the chemical variations that have been observed for minerals within the group. The transition metals found to substitute for Fe in melanterite from the Richmond mine are Cu and Zn. Natural melanterite with significant Cu contents has been reported by Keating & Berry (1953) [$(Fe_{0.53}Cu_{0.44}Zn_{0.02})SO_4 \cdot 7H_2O$] and by Palache *et al.* (1951) [$(Fe_{0.67}Cu_{0.33})SO_4 \cdot 7H_2O$]. In a study of the synthetic system $CuSO_4$–$FeSO_4$–H_2O, Collins (1923) observed the upper limit of iron-for-copper substitution in ferroan boothite to be $(Cu_{0.66}Fe_{0.34})SO_4 \cdot 7H_2O$. The end-member boothite, $CuSO_4 \cdot 7H_2O$, is rare, and the natural occurrence of this mineral has even been questioned. Optical and morphological data are given in Palache *et al.* (1951) for boothite that dehydrated to chalcanthite ($CuSO_4 \cdot 5H_2O$). Zinc-melanterite ($Zn_{0.57}Fe_{0.35}Mg_{0.097}Ca_{0.021})SO_4 \cdot 7H_2O$ has been described by Liu *et al.* (1995).

Method of Synthesis

The synthetic melanterite samples provided by Bodurtha (1995) were grown in an anaerobic glove-box containing an argon atmosphere with 2.5% hydrogen gas. A low concentration of O_2 was verified using commercial methylene blue indicator strips. Commercial $FeSO_4 \cdot 7H_2O$ and $CuSO_4 \cdot 5H_2O$ were dissolved in 0.1M H_2SO_4 at 50°C in various proportions, and an iron wire was added to the solution to enhance reduction of Fe^{3+}. Sulfuric acid was added until the solution was saturated. The solution was filtered and allowed to cool to 22°C in the glove box. The solution was decanted, by vacuum filtering, and the resulting crystals were left to dry overnight in the glove box, on the filter paper. Samples melant8(100), m10b, n73 and m40a were synthesized in this way.

Chemical Analysis

Melanterite from Iron Mountain was analyzed for Fe, Cu and Zn with an electron microprobe. Chips of coarsely crystalline melanterite (Fig. 5) were surrounded by epoxy in glass tubes 1 cm in diameter and were polished in oil. The electron beam, with a beam current of approximately 20 nA at 15 kV, was rastered over an area 0.1 × 0.1 mm to minimize sample damage over the 200 seconds of collection time. Chalcopyrite (S–332 Queen's Univ.) and sphalerite (S–334 Queen's Univ.) were used as standards. The melanterite is very difficult to analyze, as fluid inclusions burst because of the vacuum and heating by the electron beam. The resulting fluid and gas destroy the carbon coating. The samples had been stored in mineral oil since they were collected; under vacuum, the oil slowly seeped out of the grains and disrupted the carbon coating. Only Fe, Cu and Zn and S were observed; the low signal-to-noise ratio resulted in poor detection-limits as a result of the degradation of the sample surface during analysis.

An analysis for Fe, Cu and Zn by inductively coupled plasma – mass spectrometry was conducted on natural specimens of melanterite from Iron Mountain, for which large homogeneous fragments were available. Synthetic melanterite was analyzed for Fe and Cu by dissolution of the crystals and measurement of the solution concentration by atomic absorption spectroscopy. Standard solutions of $FeSO_4$ and $CuSO_4$ were studied for comparison. Table 1 contains a summary of the chemical composition, cell dimensions and agreement factors of

FIG. 2. Stalactites of melanterite hanging from a water pipe in the Richmond adit about 200 m in from the portal and close to where the adit approaches the nearby Mattie deposit.

the synthetic and natural melanterite samples for which the atomic structure was refined.

RESULTS OF CHEMICAL ANALYSIS

The compositions of the melanterite (Fig. 6) illustrate the variability of the metal ratios within the deposit. The melanterite shows a wide range of composition that varies from the Fe end-member to those with equal amounts of Fe, Cu and Zn. Most samples are classified as melanterite, but sample 91RS209c (Table 1) is zinc-melanterite $(Zn_{0.62}Fe_{0.34}Cu_{0.04})SO_4 \cdot 7H_2O$. The atomic structure of zinc-melanterite is reported here. The zinc content of this material exceeds the limit of Zn-for-Fe substitution suggested by Jambor *et al.* (2000). This extra substitution of Zn may be made possible by the

FIG. 3. Smaller stalactites of melanterite forming on a ventilation tube in the same area as those shown in Figure 2. The stalactites are commonly hollow, 3–5 mm in inner diameter, through which fluids pass downward and deposit melanterite at the termination. The stalactite near the scale is an example of such a "drinking straw" morphology.

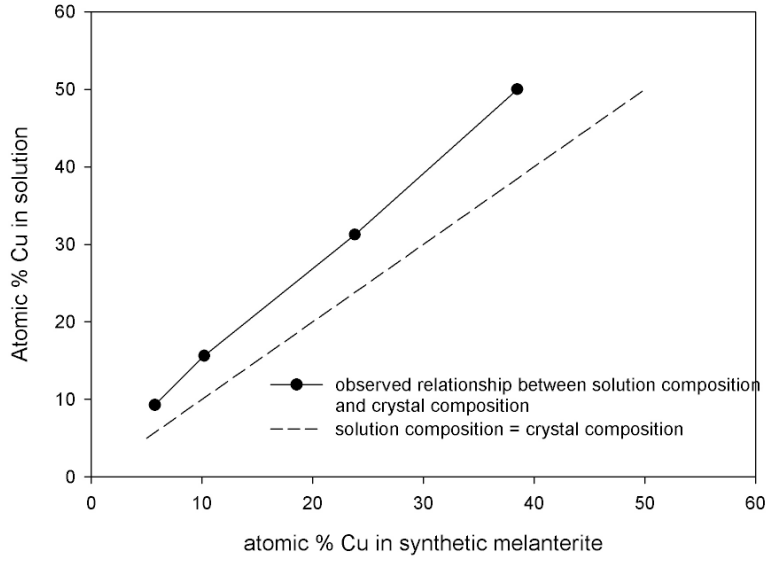

FIG. 4. Synthetic precipitates of Cu-bearing melanterite are depleted in Cu relative to the solution from which they crystallize.

TABLE 1. CHEMICAL COMPOSITION (MOLE %), AGREEMENT FACTORS AND UNIT-CELL DIMENSIONS FOR SYNTHETIC MELANTERITE (SYN) AMD MELANTERITE FROM IRON MOUNTAIN (IM), CALIFORNIA

Sample		Cu	Zn	Fe	method	# refl	R	wR	*a* (Å)	*b* (Å)	*c* (Å)	β (°)	volume (Å^3)
melant8(100)	syn	0.00	0.00	100.00	AA	2815	0.088	0.077	14.04(1)	6.502(2)	10.952(6)	105.81(6)	962.0(10)
Baur (1964)	syn	0.00	0.00	100.00					14.07(1)	6.503(7)	11.040(10)	105.60(1)	974.0
m10b	syn	10.00	0.00	90.00	AA	2799	0.084	0.055	14.060(3)	6.505(3)	10.943(7)	105.75(5)	963.3(10)
98-rp-53	IM	20.75	2.49	76.76	ICP–MS	2293	0.062	0.050	14.071(6)	6.505(2)	10.958(3)	105.69(1)	965.7(6)
n73	syn	24.00	0.00	76.00	AA	761	0.068	0.061	14.079(6)	6.505(3)	10.947(9)	105.77(4)	964.8(10)
m2(29-rp)	IM	8.60	26.23	65.16	ICP–MS	2327	0.060	0.048	14.081(3)	6.510(1)	10.997(3)	105.63(1)	970.8(4)
m40a	syn	39.00	0.00	61.00	AA	1688	0.064	0.048	14.077(6)	6.497(3)	10.949(6)	105.81(4)	963.5(10)
98-rp-36	IM	6.99	32.42	60.59	ICP–MS	2287	0.084	0.117	14.052(3)	6.496(1)	11.026(5)	105.61(1)	969.3(3)
98-rp-mati19	IM	22.50	21.65	55.84	ICP–MS	2278	0.061	0.058	14.080(4)	6.498(2)	10.955(3)	105.65(1)	965.0(5)
mati-6	IM	10.15	41.58	48.25	ICP–MS	2276	0.060	0.059	14.073(3)	6.510(2)	10.954(3)	105.62(5)	966.5(4)
mati-7 (27-rp)	IM	34.10	30.60	35.28	ICP–MS	2224	0.068	0.051	14.100(2)	6.518(1)	10.886(2)	105.76(2)	962.9(3)
91rs209c	IM	3.97	61.60	34.42	ICP–MS	2277	0.058	0.059	14.066(3)	6.506(1)	10.938(2)	105.58(1)	964.1(4)

AA: atomic absorption, ICP–MS: inductively coupled plasma – mass spectrometry.
$R = \Sigma(|F_o| - |F_c|) / \Sigma |F_o|$, $wR = (\Sigma w(|F_o| - |F_c|)^2 / (\Sigma w|F_o|^2))^{1/2}$.

FIG. 5. The variation in color exhibited by melanterite from the Richmond mine. The material shown is the source of crystal fragments used in the X-ray-diffraction experiments. The sample numbers shown are used throughout the paper. The sample vials are 1 cm in diameter.

square-planar distortion of the *M*2 octahedron of the structure caused by Cu substitution (see below). No analyzed samples fall within the field of boothite.

The relationship between the composition of the melanterite and the location within the mine workings also is presented in Figure 6. The compositional variation of a melanterite sample is not strongly dependent on location within the mine. The widest variation occurs for materials collected from the Mattie location. All of the specimens from this location were collected within only a few meters of one another, where the Richmond mine adit passes the nearby Mattie deposit (the projection of the Mattie deposit onto the plane of the Richmond adit is denoted by x in Fig. 1b). The higher Cu and Zn values for these samples likely result from the higher overall Cu and Zn content of the Mattie de-

posit relative to the Richmond mine. However, at the Mattie location, cuprian melanterite occurs in close proximity to melanterite with an end-member composition. This extreme variation in composition within a short distance is a consequence of the heterogeneous nature of the solutions that percolate through the deposit.

The Color of Melanterite

The color variation in melanterite from the Richmond mine is striking (Figs. 2, 3, 5). Figure 7 presents the color of the material as a function of chemical composition in the system Fe–Cu–Zn. There is no obvious relationship between composition and color. For example, green or turquoise material can be very rich in Fe or have almost equal proportions of Fe, Cu and Zn. The turquoise color may be caused by only a small amount of Cu. Sample 98–RP–36 (Table 1) has only 7 at.% Cu and exhibits a turquoise color (Fig. 5). Sample Mati–7 has equal amounts of Fe, Cu and Zn and exhibits a deep blue color (Fig. 5). This deep blue color has caused melanterite to be commonly misidentified as chalcanthite during field studies.

There is a suggestion that melanterite with a yellowish color from the Richmond mine may be more zinc-rich. It is possible that minute amounts of Fe^{3+} may cause such a yellowish coloration, but no data are available as to the possible extent of Fe^{3+} incorporation in these materials. The melanterite does occur in proximity to Fe^{3+}-bearing phases such as copiapite at the Richmond mine (Fig. 8) and other locations worldwide.

A large single crystal of melanterite from a stalactite from the Richmond mine was oriented using a spindle stage and the observed cleavages, and cut into sections. All of this work was accomplished with the material immersed in mineral oil to limit dehydration The optical transmission spectra were measured. These data were collected by Professor George Rossman of California Institute of Technology and are available in electronic form at http://minerals.gps.caltech.edu/. The spectra confirm that iron is present as Fe^{2+}, H_2O is present in the structure, and there is a weak dichroism that is consistent with Fe^{2+} occupying the distorted *M*1 and *M*2 octahedra that exist in melanterite.

Structure Analysis

X-ray-diffraction data (Mo$K\alpha$ radiation) for synthetic samples melant8(100), m10b, n73 and m40a were collected using an Enraf–Nonius CAD4 diffractometer. The Iron Mountain samples listed in Table 1 were studied with a Bruker AXS diffractometer. Each crystal fragment was mounted in a 0.3 mm capillary filled with mineral oil to limit dehydration. The unit-cell dimensions (Table 1) were determined by the automatic centering of 25 reflections. Data reduction and least-squares

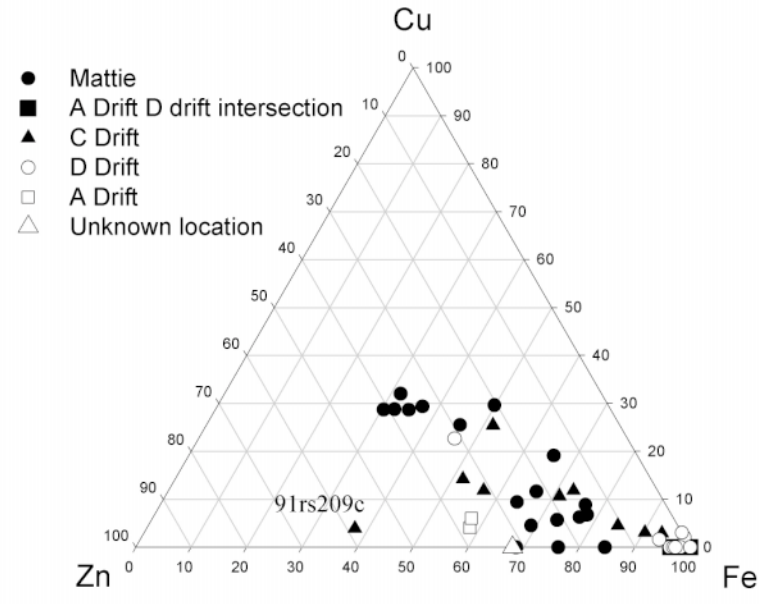

FIG. 6. The atomic proportion of Fe, Cu and Zn found in melanterite at the Richmond mine, as determined by electron-microprobe analysis and ICP–MS analysis. The composition of the zinc-melanterite is indicated by sample number 91rs209c.

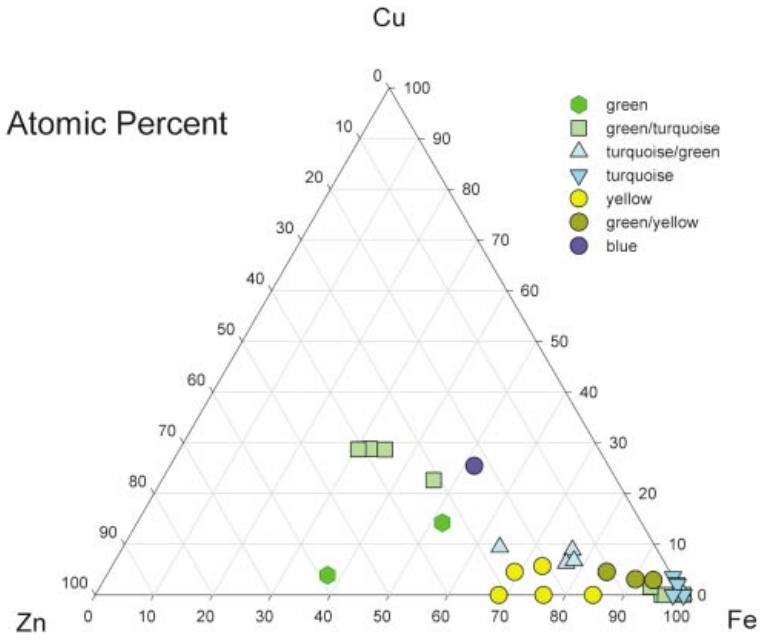

FIG. 7. The variation in color as a function of composition. There is a general trend for more Fe-rich samples to be yellow or green, and more Cu-rich samples to be blue or turquoise, but there are several exceptions to this trend.

refinement in space group $P2_1/c$ were performed with the XTAL3.0 system (Hall 2000). Agreement factors are reported in Table 1. Starting parameters were taken from Baur (1964). The metal sites were assumed to be completely filled and were modeled using the scattering factors for Fe. Site refinements of the Fe, Cu and Zn content were not possible because of the similar scattering-factors of these three elements. Table 2 lists the atom coordinates and isotropic displacement factors. The anisotropic atomic-displacement parameters and observed and calculated structure-factors are available from the Depository of Unpublished Data, CISTI, National Research Council of Canada, Ottawa, Ontario K1A 0S2, Canada.

The structure of melanterite (Fig. 9) consists of two distinct MO_6 octahedra and a sulfate tetrahedron that are linked by hydrogen bonds. All of the oxygen atoms in the structure coordinate either a metal site or the sulfur site, except for one H_2O molecule (Ow11) that is not involved directly in a coordination polyhedron. In Table 3, the bond lengths are listed for the various compositions studied. The bond lengths for synthetic melanterite determined by Baur (1964), also presented, are in excellent agreement with the synthetic melanterite melant8(100) of this study. Fronczek *et al.* (2001) described the melanterite structure measured at 120 K. The geometry of the sulfate tetrahedron does not change upon replacement of Fe by Cu, nor does the degree of distortion of the *M*1 site. A plot of the variance of the octahedron bond-lengths (Fig.10) for *M*1 shows the variance to remain constant for different bulk-compositions. However, the variances of the bond-lengths of the *M*2 octahedra show a significant increase as the Cu content of the material increases. Inspection of Table 3 reveals that this increased variance is a result of the *M*2–Ow10 bond, which becomes longer as the melanterite becomes richer in Cu. This increase is the result of the square-planar distortion induced in the *M*2 octahedron by the d^9 configuration of Cu^{2+} (Strens 1966). The length of the *M*2–Ow10 bond in cuprian melanterite is greater than that in copper-poor melanterite.

The distortion of the structure upon substitution of Cu also plays a role in the dehydration behavior of melanterite. Where only a small amount of Cu is present in the structure, the melanterite dehydrates to siderotil instead of rozenite. This change in dehydration behavior could be the result of an enhanced stability of siderotil with a small amount of Cu, with respect to rozenite. It may also be that a small amount of Cu changes the mechanism of dehydration to favor a process that produces metastable siderotil. The distortion of the atomic structure with Cu substitution may also change the limits of substitution of other metals in melanterite and explain why the zinc-melanterite from

Iron Mountain contains more Zn than has been observed previously.

Conclusions and Future Work

The melanterite group of minerals are common in acidic mine-waste systems. The structure of melanterite is able to incorporate a wide range of transition metals. The composition of melanterite that precipitates or dissolves within mine wastes, in terms of the transition metals, can dramatically change the composition of water draining from these areas. The observed limit of Cu substitution, approximately 35 at.% for material from the Richmond mine, reflects the composition of the liquids that are forming the melanterite and is not a limit imposed by crystal-chemical considerations. The present work indicates that Cu substitution takes place only at the *M*2 site. Increased substitution of Cu above a Cu:Fe ratio of 1:1 must involve Cu replacing Fe at the *M*1 site. The Jahn–Teller distortions induced at the *M*1

FIG. 8. Melanterite (dark blue) is closely associated with copiapite (yellow) on the adit walls of the Richmond mine.

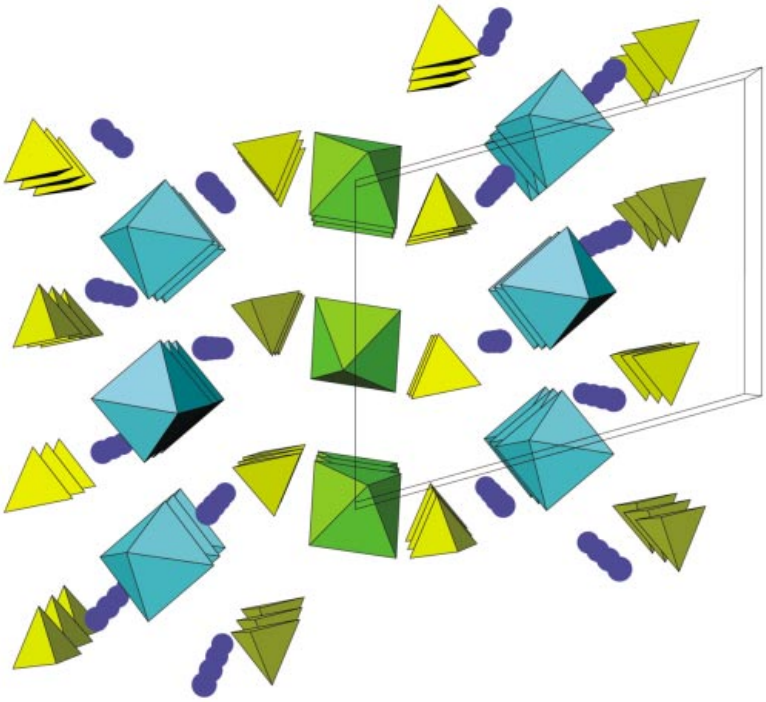

FIG. 9. The atomic structure of melanterite viewed down the *b* axis (ATOMS version 3.1; Dowty 1995). The *M*1 octahedra are green, and the *M*2 octahedra, which incorporate Cu, are blue. The structure is held together by hydrogen bonds between oxygen atoms of the sulfate tetrahedra and oxygen atoms coordinating the *M* sites. The seventh H_2O of the formula (Ow11) does not coordinate a metal or sulfur site; its presence is indicated by the isolated blue spheres.

site by Cu substitution may destabilize the structure and explain why boothite and ferroan boothite are rarely observed.

Current research into metal-site occupancies, the pattern of hydrogen bonding (Anderson 2002) and hydration–dehydration behavior as a function of temperature and composition in deuterated melanterite will give additional useful information to help in understanding the role of melanterite in problems related to acid mine-drainage.

ACKNOWLEDGEMENTS

I thank Charles Alpers, Heather Jamieson, Peter Roeder, Clare Robinson, Paul Bodurtha, George Rossman and Don Chipley for their support of this project. The manuscript was improved by the careful reviews by John L. Jambor and an anonymous reviewer, as well as the editorial assistance of Mati Raudsepp and Robert F. Martin. An NSERC operating grant to RCP funded the research.

REFERENCES

ALPERS, C.N., BLOWES, D.W., NORDSTROM, D.K. & JAMBOR, J.L. (1994a): Secondary minerals and acid-mine water chemistry. *In* The Environmental Geochemistry of Sulfide Mine-Wastes (J.L. Jambor & D.W. Blowes, eds.). *Mineral. Assoc. Can., Short Course Handbook* **22**, 247-270.

_____, NORDSTROM, D.K. & BURCHARD, J.M. (1992): Compilation and interpretation of water-quality and discharge data for acidic mine waters at Iron Mountain, Shasta County, California, 1940–91. *U.S. Geol. Surv., Water Resources Invest. Rep.* **91–4160**.

_____, _____ & THOMPSON, J.M. (1994b): Seasonal variations of Zn/Cu ratios in acid mine water from Iron Mountain, California. *In* Environmental Geochemistry of Sulfide Oxidation (C.N. Alpers & D.W. Blowes, eds.). *Am. Chem. Soc., Symp. Ser.* **550**, 324-344.

ANDERSON, J. (2002): *Hydrogen Bonding in Melanterite.* M.Sc. thesis, Queen's Univ., Kingston, Ontario.

TABLE 2. ATOM COORDINATES AND ISOTROPIC DISPLACEMENT PARAMETERS OF SYNTHETIC MELANTERITE AND MELANTERITE FROM THE RICHMOND MINE, IRON MOUNTAIN, CALIFORNIA

		melant8	M10b	98-rp-53	n73	m2	m40a	98-rp-36	mati-19	mati-6	mati-7	91rs209c
*M*1	*U*(equiv)	0.021	0.021	0.030	0.023	0.027	0.029	0.016	0.029	0.028	0.028	0.029
*M*2	*U*(equiv)	0.021	0.020	0.024	0.017	0.025	0.018	0.016	0.024	0.021	0.020	0.021
S	*x*	0.7732(1)	0.7730(1)	0.7721(1)	0.7725(2)	0.7727(1)	0.7710(1)	0.7729(1)	0.7725(1)	0.7727(1)	0.7718(1)	0.7727(1)
	y	-0.0289(2)	-0.0296(2)	-0.0316(2)	-0.0322(4)	-0.0294(2)	-0.0352(2)	-0.0301(3)	-0.0307(2)	-0.0298(2)	-0.0331(2)	-0.0284(2)
	z	0.3237(1)	0.3241(1)	0.3246(1)	0.3245(3)	0.3241(1)	0.3250(1)	0.3239(2)	0.3244(1)	0.3239(1)	0.3251(1)	0.3236(1)
	U(equiv)	0.019	0.021	0.028	0.023	0.030	0.029	0.015	0.029	0.028	0.029	0.028
O1	*x*	0.7960(3)	0.7954(3)	0.7961(2)	0.7951(6)	0.7958(2)	0.7963(3)	0.7948(4)	0.7971(2)	0.7965(3)	0.7979(2)	0.7956(2)
	y	-0.0293(5)	-0.0298(6)	-0.0318(5)	-0.0319(9)	-0.0297(4)	-0.0366(6)	-0.0324(9)	-0.0314(4)	-0.0299(5)	-0.0332(5)	-0.0280(4)
	z	0.4638(3)	0.4642(3)	0.4646(3)	0.4646(7)	0.4637(3)	0.4651(3)	0.4639(6)	0.4650(3)	0.4645(3)	0.4665(3)	0.4650(2)
	U(equiv)	0.029	0.029	0.036	0.028	0.039	0.037	0.024	0.036	0.037	0.038	0.038
O2	*x*	0.8634(3)	0.8628(2)	0.8598(2)	0.8591(6)	0.8614(2)	0.8562(3)	0.8637(4)	0.8610(2)	0.8607(3)	0.8580(2)	0.8605(2)
	y	0.0368(5)	0.0369(6)	0.0381(5)	0.037(1)	0.0387(4)	0.0397(5)	0.0381(9)	0.0390(5)	0.0403(5)	0.0388(5)	0.0418(5)
	z	0.2891(4)	0.2887(3)	0.2865(3)	0.2865(7)	0.2874(3)	0.2837(4)	0.2869(6)	0.2875(3)	0.2866(3)	0.2845(3)	0.2855(3)
	U(equiv)	0.030	0.031	0.042	0.037	0.044	0.046	0.026	0.041	0.043	0.044	0.043
O3	*x*	0.6918(3)	0.6908(3)	0.6895(2)	0.6904(6)	0.6900(2)	0.6879(3)	0.6915(4)	0.6898(2)	0.6895(3)	0.6875(2)	0.6900(2)
	y	0.1160(5)	0.1148(6)	0.1103(5)	0.1062(9)	0.1121(5)	0.1027(5)	0.1171(9)	0.1115(5)	0.1125(5)	0.1050(5)	0.1121(5)
	z	0.2727(4)	0.2733(4)	0.2745(3)	0.2730(7)	0.2725(3)	0.2768(4)	0.2747(6)	0.2741(3)	0.2730(3)	0.2754(3)	0.2720(3)
	U(equiv)	0.031	0.037	0.0411	0.035	0.044	0.042	0.025	0.042	0.042	0.044	0.042
O4	*x*	0.7447(3)	0.7459(3)	0.7457(2)	0.7445(6)	0.7452(2)	0.7464(3)	0.7445(4)	0.7458(2)	0.7463(3)	0.7462(2)	0.7464(2)
	y	-0.2360(5)	-0.2393(6)	-0.2406(5)	-0.242(10)	-0.2386(4)	-0.2423(5)	-0.2365(9)	-0.2395(5)	-0.2388(5)	-0.2424(5)	-0.2386(4)
	z	0.2736(4)	0.2748(3)	0.2755(3)	0.2757(8)	0.2737(3)	0.2749(4)	0.2751(6)	0.2757(3)	0.2749(3)	0.2749(3)	0.2748(3)
	U(equiv)	0.033	0.031	0.039	0.037	0.044	0.041	0.026	0.039	0.041	0.042	0.041
Ow5	*x*	-0.1117(3)	-0.1130(3)	-0.1129(3)	-0.1105(7)	-0.1123(2)	-0.1127(3)	-0.1128(5)	-0.1132(2)	-0.1118(3)	-0.1119(2)	-0.1112(3)
	y	-0.1170(6)	-0.1152(7)	-0.1164(5)	-0.110(1)	-0.1167(5)	-0.1119(6)	-0.120(1)	-0.1136(6)	-0.1181(6)	-0.1132(6)	-0.1186(5)
	z	0.0688(4)	0.0689(4)	0.0703(3)	0.0719(8)	0.0702(3)	0.0701(4)	0.0712(7)	0.0696(3)	0.0696(3)	0.0698(3)	0.0701(3)
	U(equiv)	0.052	0.050	0.056	0.058	0.062	0.063	0.042	0.060	0.060	0.065	0.064
Ow6	*x*	0.1008(3)	0.1026(3)	0.1017(2)	0.0994(6)	0.1011(2)	0.1016(3)	0.1006(5)	0.1009(2)	0.1006(3)	0.1008(3)	0.0996(2)
	y	-0.0443(6)	-0.0435(6)	-0.0450(5)	-0.0431(9)	-0.0437(4)	-0.0447(5)	-0.0466(9)	-0.0435(5)	-0.0439(5)	-0.0448(5)	-0.0423(5)
	z	0.1830(4)	0.1836(3)	0.1832(3)	0.1838(7)	0.1822(3)	0.1841(4)	0.1858(6)	0.1827(3)	0.1830(3)	0.1825(3)	0.1803(3)
	U(equiv)	0.034	0.036	0.042	0.037	0.044	0.047	0.029	0.044	0.044	0.046	0.044
Ow7	*x*	-0.0306(3)	-0.0304(3)	-0.0293 (2)	-0.0292(6)	-0.0290(2)	-0.0284(3)	-0.0307(4)	-0.0292(2)	-0.0294(3)	-0.0283(2)	-0.0297(2)
	y	0.2964(5)	0.2958(6)	0.2967(5)	0.2974(9)	0.2961(4)	0.2983(5)	0.2936(9)	0.2945(4)	0.2956(5)	0.2960(5)	0.2933(4)
	z	0.0679(4)	0.0669(4)	0.0679(3)	0.0681(8)	0.0683(3)	0.0686(4)	0.0692(6)	0.0692(3)	0.0685(3)	0.0692(3)	0.0676(3)
	U(equiv)	0.030	0.032	0.039	0.036	0.043	0.045	0.023	0.039	0.040	0.044	0.041
Ow8	*x*	0.5198(3)	0.5207(3)	0.5194(2)	0.5196(6)	0.5195(2)	0.5183(3)	0.5205(4)	0.5198(2)	0.5192(3)	0.5186(2)	0.5199(2)
	y	-0.0427(6)	-0.0415(6)	-0.0442(5)	-0.046(1)	-0.0423(4)	-0.0485(5)	-0.0440(9)	-0.0444(5)	-0.0464(5)	-0.0489(5)	-0.0465(4)
	z	0.3193(3)	0.3197(3)	0.3221(3)	0.3236(7)	0.3203(3)	0.3264(4)	0.3193(6)	0.3216(3)	0.3213(3)	0.3238(3)	0.3210(3)
	U(equiv)	0.032	0.039	0.040	0.034	0.042	0.042	0.028	0.042	0.041	0.041	0.040
Ow9	*x*	0.4311(3)	0.4299(3)	0.4304(2)	0.4306(6)	0.4309(2)	0.4295(3)	0.4303(5)	0.4305(2)	0.4316(3)	0.4309(2)	0.4319(2)
	y	0.2862(5)	0.2840(6)	0.2761(5)	0.277(1)	0.2817(4)	0.2639(6)	0.2831(9)	0.2767(5)	0.2788(5)	0.2683(5)	0.2819(4)
	z	0.4411(4)	0.4417(4)	0.4410(3)	0.4419(8)	0.4416(3)	0.4400(4)	0.4410(6)	0.4409(3)	0.4415(3)	0.4403(3)	0.4416(3)
	U(equiv)	0.033	0.035	0.042	0.036	0.044	0.047	0.027	0.043	0.042	0.044	0.043
Ow10	*x*	0.3534(3)	0.3527(3)	0.3502(2)	0.3502(6)	0.3528(2)	0.3465(3)	0.3525(4)	0.3519(2)	0.3533(3)	0.3491(2)	0.3546(2)
	y	-0.1407(6)	-0.1447(7)	-0.1515(5)	-0.148(1)	-0.1452(5)	-0.1626(6)	-0.1422(9)	-0.1483(5)	-0.1453(6)	-0.1580(5)	-0.1425(5)
	z	0.4401(4)	0.4399(4)	0.4409(3)	0.4396(7)	0.4402(3)	0.4419(4)	0.4417(6)	0.4408(3)	0.4411(3)	0.4407(3)	0.4413(3)
	U(equiv)	0.033	0.035	0.042	0.036	0.045	0.046	0.026	0.044	0.042	0.046	0.041
Ow11	*x*	0.3632(3)	0.3637(3)	0.3656(2)	0.3656(6)	0.3649(2)	0.3691(3)	0.3631(5)	0.3652(2)	0.3645(3)	0.3676(2)	0.3641(2)
	y	0.0056(5)	0.0047(6)	0.0070(5)	0.009(1)	0.0055(4)	0.0086(5)	0.0047(9)	0.0064(5)	0.0057(5)	0.0088(5)	0.0052(4)
	z	0.1148(4)	0.1140(3)	0.1135(3)	0.1139(7)	0.1152(3)	0.1131(4)	0.1133(6)	0.1148(3)	0.1156(3)	0.1148(3)	0.1163(3)
	U(equiv)	0.036	0.034	0.041	0.038	0.045	0.041	0.031	0.043	0.042	0.044	0.042

*M*1 and *M*2 are located at 0,0,0 and ½,0,½.

BAUR, W.H. (1964): On the crystal chemistry of salt hydrates. III. The determination of the crystal structure of $FeSO_4 \cdot 7H_2O$ (melanterite). *Acta Crystallogr.* **17**, 1167-1174.

BODURTHA, P. (1995): *A Geochemical-Mineralogical Study of Melanterite $FeSO_4 \cdot 7H_2O$*. BSc. thesis, Queen's Univ., Kingston, Ontario.

COLLINS, H.F. (1923): On some crystallized sulphates from the province of Huelva, Spain. *Mineral. Mag.* **20**, 32-38.

DOWTY, E.(1995): ATOMS version 3.1. Shape Software, 521 Hidden Valley Road, Kingsport, Tennessee 37663, U.S.A. http://www.shapesoftware.com/

FRAU, F. (2000): The formation–dissolution–precipitation cycle of melanterite at the abandoned pyrite mine of Genna Luas in Sardinia, Italy: environmental implications. *Mineral. Mag.* **64**, 995-1006.

TABLE 3. BOND LENGTHS (Å) OF SYNTHETIC MELANTERITE AND MELANTERITE FROM THE RICHMOND MINE, IRON MOUNTAIN, CALIFORNIA

Sample	*M*1-Ow5	*M*1-Ow6	*M*1-Ow7	mean	variance	*M*2-Ow8	*M*2-Ow9	*M*2-Ow10	mean	variance	S-O1	S-O2	S-O3	S-O4	mean
melant8(100)	2.062(5)	2.135(4)	2.150(4)	2.116	0.0015	2.091(4)	2.115(4)	2.183(4)	2.130	0.0015	1.479(4)	1.480(4)	1.468(4)	1.468(3)	1.474
Baur(1964)	2.068(5)	2.144(5)	2.136(5)	2.116	0.0012	2.096(5)	2.109(5)	2.188(5)	2.131	0.0017	1.488(4)	1.481(4)	1.466(4)	1.462(4)	1.474
m10b	2.074(5)	2.151(3)	2.142(4)	2.122	0.0012	2.089(4)	2.109(4)	2.206(4)	2.135	0.0026	1.479(3)	1.481(4)	1.476(4)	1.479(4)	1.479
98-rp-53	2.086(4)	2.147(3)	2.148(3)	2.127	0.0008	2.061(3)	2.064(3)	2.258(3)	2.128	0.0085	1.479(3)	1.477(3)	1.470(3)	1.473(3)	1.475
n73	2.050(9)	2.134(7)	2.153(7)	2.112	0.0020	2.045(9)	2.064(7)	2.248(8)	2.119	0.0084	1.479(8)	1.463(9)	1.453(7)	1.482(7)	1.469
m2(29-rp)	2.081(4)	2.141(3)	2.148(3)	2.123	0.0009	2.085(3)	2.094(3)	2.211(3)	2.130	0.0033	1.481(3)	1.480(4)	1.474(3)	1.482(3)	1.479
m40a	2.073(5)	2.150(4)	2.155(4)	2.126	0.0014	2.011(4)	2.000(4)	2.333(4)	2.115	0.0239	1.477(4)	1.474(5)	1.454(4)	1.459(4)	1.466
98-rp-36	2.099(8)	2.174(6)	2.141(6)	2.138	0.0009	2.107(7)	2.103(6)	2.202(6)	2.137	0.0021	1.490(6)	1.506(7)	1.479(6)	1.459(6)	1.484
98-rp-mati19	2.078(4)	2.138(3)	2.138(3)	2.118	0.0008	2.067(3)	2.066(3)	2.229(3)	2.121	0.0058	1.485(3)	1.481(3)	1.472(3)	1.469(3)	1.477
mati-6	2.072(4)	2.139(3)	2.146(3)	2.119	0.0011	2.069(3)	2.074(3)	2.203(3)	2.115	0.0038	1.486(3)	1.477(4)	1.479(3)	1.473(3)	1.479
mati-7 (27-rp)	2.064(4)	2.126(3)	2.148(3)	2.113	0.0013	2.031(3)	2.021(3)	2.293(3)	2.115	0.0159	1.482(3)	1.479(4)	1.472(3)	1.478(3)	1.458
91rs209c	2.067(4)	2.108(3)	2.128(3)	2.101	0.0006	2.073(3)	2.088(3)	2.179(3)	2.113	0.0022	1.493(2)	1.478(3)	1.468(3)	1.478(3)	1.479

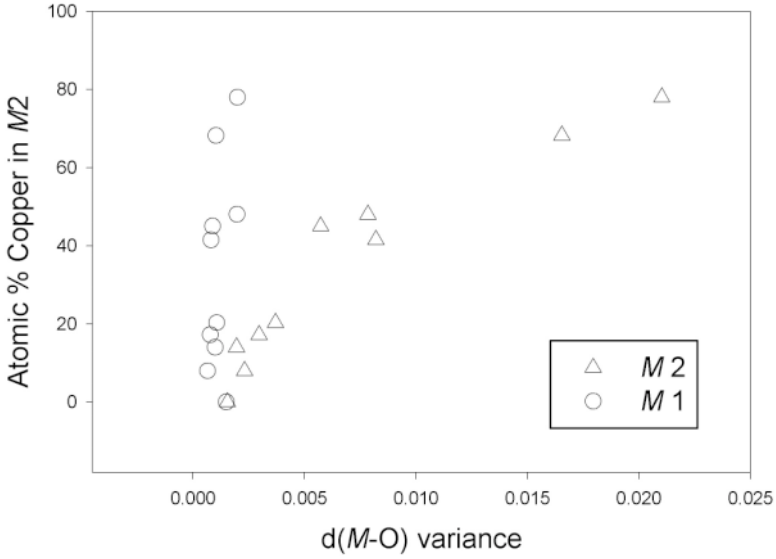

FIG. 10. As Cu^{2+} substitutes for Fe^{2+} at the *M*2 site, the distortion of the octahedron increases, as measured by the bond variance. This increase in bond variance is a result of the square-planar distortion induced by Cu^{2+}. The ion Cu^{2+} has a d^9 configuration, which leads to a Jahn–Teller distortion (Strens 1966) in the *M*2 octahedron. The *M*2–O10 bond becomes much longer than the *M*2–Ow8 and *M*2–Ow9 bonds as Cu^{2+} is substituted into the octahedron (Table 3). No square-planar distortion is observed for the *M*1 octahedron. The vertical axis of the graph refers to the Cu content of the *M*2 octahedron; all the Cu determined by chemical analysis is assumed to occur at *M*2. The distortion of the corresponding *M*1 is plotted for comparison, but the *M*1 site is assumed to be free of Cu. The y coordinate of the *M*1 data points are those of the corresponding points for *M*2, and have no bearing on the scale along the vertical axis.

FRONCZEK, F.R., COLLINS, S.N. & CHAN, J. (2001): Refinement of ferrous sulfate heptahydrate (melanterite) with low-temperature CCD data. *Acta Crystallogr.* **E57**, i26-27.

GAINES, R.V., SKINNER, H.C.W., FOORD, E.E., MASON, B. & ROSENZWEIG, A. (1997): *Dana's New Mineralogy* (eighth ed.). John Wiley and Sons, New York, N.Y.

HALL, S.R. (2000): *The Xtal System*. The University of Western Australia, Nedlands, 6907, W.A., Australia.

HAWTHORNE, F.C., KRIVOVICHEV, S.V. & BURNS, P.C. (2000): The crystal chemistry of sulfate minerals. *In* Sulfate Minerals – Crystallography, Geochemistry and Environmental Significance (C.N. Alpers, J.L. Jambor & D.K. Nordstrom, eds.). *Rev. Mineral. Geochem.* **40**, 1-112.

JAMBOR, J.L., NORDSTROM, D.K. & ALPERS, C.N. (2000): Metal-sulfate salts from sulfide oxidation. *In* Sulfate Minerals – Crystallography, Geochemistry and Environmental Significance (C.N. Alpers, J.L. Jambor, D.K. Nordstrom, eds.). *Rev. Mineral. Geochem.* **40**, 303-350.

KEATING, L.F. & BERRY, L.G. (1953): Pisanite from Flin Flon, Manitoba. *Am. Mineral.* **38**, 501-505.

LIU TIEGEN, GONG GUOHONG & YE LIN (1995): Discovery and investigation of zinc-melaterite (*sic*) in nature. *Acta Mineral. Sinica* **15**, 286-290 (abstr. in *Am. Mineral.* **81**, 1518).

NORDSTROM, D.K & ALPERS, C.N. (1999): Negative pH, efflorescent mineralogy and consequences for environment restoration at the Iron Mountain superfund site, California. *In* Geology, Mineralogy and Human Welfare (J.V. Smith, P.R. Buseck & M. Ross, eds.). *Proc. Nat. Acad. Sci.* **96**, 3455-3462.

_____, _____, PTACEK, C.J. & BLOWES, D.W. (2000): Negative pH and extremely acidic mine waters from Iron Mountain, California. *Environ. Sci. Technol.* **34**, 254-258.

PALACHE, C., BERMAN, H.& FRONDEL, C. (1951): *Dana's System of Mineralogy* **II** (seventh ed.). J. Wiley & Sons, New York, N.Y.

STRENS, R.G.J. (1966): The axial-ratio-inversion effect in Jahn–Teller distorted ML_6 octahedra in the epidote and perovskite structures. *Mineral. Mag.* **35**, 777-781.

Received June 14, 2002, revised manuscript accepted July 22, 2003.